Submitted to ADVANCED ENERGY MATERIALS

DOI: 10.1002/aenm.((please add manuscript number))
Article type: Full Paper

Title: **Linking Vertical Bulk-heterojunction Composition and Transient Photocurrent Dynamics in Organic Solar Cells with Solution-processed MoO_x Contact Layers**

Bertrand J. Tremolet de Villers, Roderick C. I. MacKenzie, Jacek J. Jasieniak, Neil Treat, Alan Heeger, and Michael Chabinyc*

((Optional Dedication))

Dr. B. J. Tremolet de Villers, N. Treat, Prof. Michael L. Chabinyc
Materials Department
University of California,
Santa Barbara, CA 93106-5050, USA
E-mail: mchabinyc@engineering.ucsb.edu

Dr. R. C. I. MacKenzie
Engineering
Room B86 Coats
University Park
Nottingham
NG7 2RD
United Kingdom

Dr. J. J. Jasieniak, Prof. A. Heeger
Center for Polymer and Organic Solids
Physics Department
University of California,
Santa Barbara, CA 93106, USA

Keywords: organic solar cells; photocurrent; drift-diffusion; metal oxide

We demonstrate how a combination of microsecond pulsed-LED transient photocurrent measurements and film morphology characterization can be used to identify a charge-carrier blocking layer within polymer:fullerene bulk-heterojunction solar cells. To do this, we use solution-processed molybdenum oxide (s-MoO_x) interlayers to control the morphology of the bulk-heterojunction. By selecting either a low- or high-temperature annealing (70°C or 150°C) for the s-MoO_x layer, we are able to fabricate a well-performing device with an ideally interconnected, high-efficiency morphology, or a device in which the PCBM phase segregates near the hole extracting contact preventing efficient extraction. With these two contrasting model systems, we then probe the photocurrent dynamics as a function of excitation voltage and

light intensity. Using dynamic secondary-ion mass spectroscopy (DSIMS), we correlate the vertical phase composition of the polymer:fullerene active layer with the optoelectronic response of the solar cells. Numerical simulations are used to verify and understand the experimental results. The result is a method to detect poor morphologies in operating organic solar cells.

1. Introduction

Organic solar cells have shown considerable promise as a low cost source of electricity [1]; however for these devices to make the transition from the laboratory to a commercial product, longer working lifetimes are still required [2]. Toward this goal, transition-metal oxides are now widely used as contact and recombination layers in organic bulk heterojunction solar cells (BHJs) [3]. It has recently been reported that replacing contact layers made of poly(3,4-ethylenedioxythiophene) poly(styrenesulfonate) (PEDOT:PSS) and low work function metals with more stable metal oxides, leads to improved lifetimes.[Ref: Steirer, K. X.; Ndione, P. F.; Widjonarko, N. E.; Lloyd, M. T.; Meyer, J.; Ratcliff, E. L.; Kahn, A.; Armstrong, N. R.; Curtis, C. J.; Ginley, D. S.; Berry, J. J.; Olson, D. C. *Adv. Funct. Mater.* **2011**, *1*, 813–820.] In many cases these metal oxide layers are deposited from solution precursors and cured at relatively low temperatures compatible with roll-to-roll fabrication techniques [4]. However, solution processing coupled with low curing temperatures produces disordered layers with uncertain optoelectronic properties. Despite these difficulties, solution-processed metal oxides have proven to form high-performance BHJs. For example, low-temperature, solution-processed molybdenum oxide (s-MoO_x) has been shown recently to form efficient BHJ solar cells with significantly-improved electrical stability.[5, 6]

In this paper, we seek to identify the relationships among the processing conditions of the metal oxide interlayer, the resulting BHJ morphology, and the photocurrent responses of the BHJ solar cells. The relationships between the processing conditions and final device performance are still difficult to predict for MoO_x and other metal oxides such as TiO_2, NiO [4,7]. In many cases, distorted (s-shaped) current-voltage characteristics are observed; the origins of which are difficult to uncover using steady-state measurements. Here we show how time-dependent electrical measurements of BHJs of P3HT:PCBM with known vertically stratification can be understood using numerical simulation. These results should be helpful for characterization of BHJs where it is difficult to measure the vertical composition using physical characterization methods.

In a previous study, we found that the shape of the steady-state current-voltage (J-V) response of a P3HT:PCBM BHJ solar cell utilizing an s-MoO_x hole-contact layer depends sensitively on the temperature used to treat the s-MoO_x.[6] In this work, we use these solar cells to study how theor transient J-V responses differ with the vertical distribution of P3HT and PCBM phases. The vertical composition is affected by heat treatent of the s-MoO_x before spin-casting the active layer. Surprisingly, the electronic structure of the s-MoO_x layer determined by ultraviolet photo-emission spectroscopy (UPS) is not significantly changed by varying the s-MoO_x annealing temperature. This result helps us isolate the substantial changes observed in the steady-state J-V curves of the solar cells to differences in the active layer morphology.[8] It is well known that device performance depends on the distribution of electron-donor and acceptor molecules within

a BHJ organic solar cell[9]. Thus, the system here provides an important model system of a vertically segregated BHJ that can be used to understand the impact of the vertical composition of the BHJ on the opto-electronic response of solar cells.

Information about the underlying physical processes defining cell operation can be gained from studying dark and light steady-state current-voltage measurements.(REFS) For example, dark J-V measurements can provide information about the ideality factor which is defined by the distribution of trap states through which recombination occurs within a device. (REFS) Similarly, light J-V curve measurements can give information on the underlying photophysical processes such as charge generation. However, more detailed information about transport and recombination processes can be obtained through transient measurements.(REFS) In recent years, several transient photocurrent techniques have been developed to investigate charge transport and recombination in OPV devices. Both Photo-generated charge extraction with a linearly-increasing voltage pulse (Photo-CELIV) and transient photovoltage techniques have been used to study recombination in OPV devices. [8, 10, 11, 12] Charge extraction (CE) and pulsed-LED transient photocurrent measurements were used by Shuttle et al. to study the role of energetic disorder, particularly in the low-energy tail of the density of states (DoS) of polymer:fullerene OPVs.[13]. While, McNeil and coworkers used pulsed-LED transient photocurrents to investigate charge trapping and transport in polymer:fullerene, polymer:polymer, and polymer:(II-VI) nanoparticle solar cells.[14, 15, 16] To best understand the results from transient experiments, it is also important to understand the structure of the BHJ layer and thereby gain information about the charge transport pathways.

Our approach here is to use solution-processed molybdenum oxide (s-MoO_x) interlayers to control the morphology of P3HT:PCBM BHJ solar cells. We fabricate two model devices, one with the MoO_x interlayer annealed at 70° C and one with the interlayer annealed at 150° C. Using DSIMS we demonstrate that when the MoOx layer is annealed at 150° C, a PCBM layer builds up at the hole extracting contact. Comparing experimental measurements and simulations of both the steady-state and transient photocurrent responses of devices with ideal and non-ideal morphologies, as affected by the s-MoO_x underlayer, we observe characteristic features of a device with charge-carrier extraction problems. Thus, we demonstrate that photocurrent signals can be used to identify poor device morphology in functioning devices.

2. Results and Discussion

2.1. Determining the Vertical Phase Composition

The s-MoO_x BHJ solar cell fabrication is depicted in **Figure 1**. An s-MoO_x layer was deposited by spin-casting MoO_x precursor solution onto clean ITO substrates. The s-MoO_x layer was then annealed at a temperature, Δ_1. In this work, we used two different s-MoO_x annealing temperatures, Δ_1 =70°C and Δ_1 =150°C. A P3HT:PCBM photo-active layer was then spin-cast onto the annealed s-MoO_x layer. An aluminum cathode was thermally deposited on top of the P3HT:PCBM and the device was subsequently annealed at Δ_2 =150°C. Full details on device fabrication can be found in the supplementry information.

The following sections might need to be modified depending on the other paper to prevent self-plagiarism, etc. I think its fine to describe the results and we will need to plot the data differently than the previous version since we will likely submit them in parallel.

Figure 2 shows the volume fraction of fullerene in the P3HT:PCBM blend film as a function of depth from the surface of the film down towards the organic/MoO_x interface as measured by DSIMS. When the s-MoO_x is treated at 70°C, the P3HT:PCBM adopts a favorable blend composition (blue trace). In this case, the DSIMS profile shows an accumulation of fullerene at the cathode/active layer interface. This is favorable because electrons are transported through the fullerene phase, therefore it is best to have as much fullerene as possible near the interface with the cathode. Further into the film, the volume fraction of PCBM decreases until the distribution of P3HT and PCBM becomes homogeneous, as represented by the flat part of the trace showing a constant fullerene volume fraction.

When the s-MoO_x is treated at 150°C, the DSIMS profile (orange trace in Figure 2) reveals the P3HT:PCBM film composition differs significantly compared to when the film is deposited onto a 70°C-treated s-MoO_x substrate, particularly at the active layer/MoO_x interface. Whilst accumulation of fullerene takes place at the top of the film near the cathode interface and the center of the film contains a constant volume fraction of each component, the composition of the film near the organic/anode interface is greatly enriched in fullerene. We found that within approximately 10nm of the 150°C-treated MoO_x/ITO substrate, the polymer:fullerene active layer is composed of up to 75% PCBM, by volume fraction. Consequently, having mostly fullerene at the anode interface represents a significant barrier to the hole extraction, as holes are primarily transported through the P3HT phase. This is likely the explanation for why the steady-state J-V curves of devices using 150°C-treated s-MoO_x show a pronounced kink (see **Figure 3**). Holes cannot be extracted from the device as easily as electrons can and therefore a significant space-charge develops within the active layer. This result is larger than observations of the J-V characteristics of intentionally placed layers of P3HT at the cathode.(need to double check my paper with Lynn Loo to see about the drop in FF at similar thickness)

2.2. Vertically Phase Separated Structures Lead to S-Shape J-V Characteristics

Devices with significant enrichment of PCBM at the s-MoO_x anode show drastically different response upon illumination than those without (Figure 3). While the device using s-MoO_x annealed at 70°C (red curves) exhibits relatively idea characteristics, a device with 150°C-treated s-MoO_x (black curves) shows s-shaped J-V curves resulting in a low fill factor (Figure 3a). Figs. 3b and 3c show how the short-circuit current density ($J_{sc)}$ and open-circuit voltage (V_{oc}), respectively, change as the light intensity is varied. As expected for a properly working solar cell, the J_{sc} should scale linearly with the light intensity. The curve fit in Fig. 3b shows $J \propto I^{\alpha}$, with $\alpha = 0.97$. At higher light intensities, e.g. I > 10% of one sun, significant deviation from linearity occurs for the device with s-MoO_x annealed at 150°C. See Table SI-1 in the Supporting Information (SI) for tabulated performance parameters–J_{sc}, V_{oc}, FF, and η_{ext} - at all light intensities.

S-shape J-V curves have been described in several other organic and hybrid organic-inorganic solar cells, including ones with P3HT:PCBM active layers.[12, 17, 18, 19, 20] However, a survey of these studies reveals that there is no single cause for the appearance of the low-fill-

factor J-V curves. Tress et al. reported that misbalance of the electron and hole mobilites is responsible for the low device performance; whereas simulations by Nelson et al. found the s-shape is sensitive to the interfacial energy offsets at the electrode/organic interfaces. Experimentally, Gupta et al. and Glatthaar et al. found the s-curve prominent upon degradation/oxidation of the low-work-function cathode. Finally, Tremolet de Villers and co-workers showed that the shape of the J-V curve can be dependent upon the vertical distribution of phases in the blend-film active layer. In our present study, we show the last effect, i.e. phase segregation, to be the dominant cause of the distorted J-V response.

Despite the differences in steady-state behavior near the open circuit voltage, the internal microstructure of the bulk of devices with low and high temperature s-MoO_x allows essentially the same charge generation efficiency in both cases. The current density for both sets of curves is roughly identical when the applied bias is large, for example when $V_{app} < -1.0$ V, but differs significantly as the applied voltage increases toward open-circuit conditions. P3HT:PCBM BHJs have not been reported to exhibit field-dependent charge generation.[21] This result therefore implies a field-dependent barrier to charge extraction exists in the "s-curve" device. In other words, holes and/or electrons cannot be collected easily at the electrodes without a large enough internal field to extract the carriers out of the active layer. Furthermore, the onset of the J-V curve "kink" shifts with light-intensity as the voltage is swept from negative to positive bias. This indicates the kink is a function of the photo-generated charge-density. Both the E-field dependence and carrier concentration effects can be explained by the presence of a charge extraction barrier that results in the buildup of one type of charge carrier in the film (holes in our case) that then creates a space-charge inhibiting current flow.

2.3. Transient Photocurrent Response

2.3.1 Light-intensity Dependence

The transient response of BHJs to illumination can reveal the dynamics of how the steady-state characteristics are reached. The transient current responses of the devices to 500-μs pulses of light from an array of red LEDs whose output is centered around 625 nm are shown in **Figure 4**. The light intensity is varied from one sun equivalent down to 10% of one sun, which varies the charge carrier concentration in the devices. The layers are kept at the same thickness which makes the geometric capacitances equivalent for the devices.

First we examine the transient response of the devices that produce J-V curves without the s-shape. For devices made with s-MoO_x sintered at 70°C, the photocurrent dynamics are mostly independent of the light intensity, as shown in Fig. 4a. Upon turn-on of the light, the photocurrent increases quickly, reaching it steady-state value within the first 25 μs. The rise and fall of the photocurrent following turn-on/turn-off of the LEDs are shown in the insets of Fig. 4a in which the photocurrent has been normalized to the mean value of the current from 450–500 μs when steady-state has been established. In the 70°C-treated s-MoO_x device, the photocurrent rise slows slightly as the light is decreased indicating a dependence of the rise on the photo-generated charge concentration. This is evidence of trap-filling as the smaller number of photo-generated charges takes longer to fill in traps encountered during the transit of charges from one end of the film to the other. In other words, some charges fall into traps as they traverse the film and steady-

state is not reached until traps are filled and trapping/de-trapping reaches steady state. When the light is turned off, the photocurrent decays quickly to zero. As is the case for the rise, the decay slows down at the lowest light intensity (10% of one sun), possibly due to less recombination in the device at low light intensity, however it is difficult to quantify and the effect is slight. That the 70°C-MoO_x photocurrent transients are mostly independent of light intensity and unremarkable in both turn-on and turn-off dynamics indicates no significant problems with charge extraction in the device.

On the contrary, the transients from solar cells using s-MoO_x treated at 150°C that have s-shaped steady state characteristics show more complex rise/fall dynamics. In Figure 4b, one sees that at one sun, the photocurrent does not rise monotonically to its steady-state value. Instead, the current quickly overshoots steady- state by ~300% at its peak, before settling down to a constant value after ~80 μs. When the excitation light intensity is reduced to 40% of one sun, an overshoot peak is also observed, albeit with a lower peak height - approximately 1.8 times the equilibrium current - and a slower recovery to steady-state. As the light intensity is further decreased to 10% of one sun, the overshoot peak is no longer present; instead, the photocurrent increases steadily to its equilibrium value, similar to the behavior of the 70°C-treated s-MoO_x device. Similar transient peaks have been observed previously in a P3HT:polyfluorene polymer blend solar cell.[31] In that case, the authors attributed that transient peak to a build-up of trapped electrons near the anode, resulting in a lower internal electric field near that interface and thus enhancing recombination and reducing exciton dissociation. Clearly many explanations for such observations are possible, but here we know through morphological measurements that excess PCBM exists at the anode and supports the claim that the peak corresponds to poor extraction of holes caused by the energetic barrier at the MoO_x/ITO interface.

2.3.2 Voltage Dependence

In addition to measuring the light intensity dependence of the pulsed photocurrent, we also investigated the effects of an applied voltage on the transient current. **Figure 5** describes the photocurrent transient response of the devices under the influence of an external voltage bias, illuminated with a light intensity equal to one sun. As before, the rise and fall of the transients are shown in absolute scale and normalized to the mean value of the current from 450–500 μs when steady-state has been established. The applied bias was varied from -1.5 to +0.5 V, thus manipulating the internal electric field within the device from one which facilitates drift of the charge carriers to their respective electrodes (at negative bias) to a field that opposes the photocurrent and brings the devices towards open-circuit conditions (around +0.5 V). Comparing the shapes of the transients for 70° C- and 150° C-MoO_x devices—Figs. 5a and 5b, respectively —one sees the former is relatively independent of bias while the latter is greatly affected by the applied electrical bias.

The early-time dynamics after turn-on and the photocurrent decay after turn-off of the excitation light are rich in information. As shown in the insets of Figure 5a, we found that for the 70°C-treated s-MoO_x device, the current always rises monotonically to its steady-state value, independent of the applied bias. Sweeping the applied bias towards a larger positive value reduces the internal electric field and causes the photocurrent rise to slow down. Similarly, the decay of the photocurrent after light turn-off retains a constant shape at all negative voltages and only changes shape when the polarity of the applied bias is switched to positive. Retarding of the

rise/fall time of the current is caused by a reduction of the electric field that slows down the drift of charges through the cell.

As was the case with varying the light intensity, changing the applied bias (but maintaining a one-sun illumination intensity) has a greater effect on the 150°C-treated s-MoO_x device. At very negative voltages, $V_{app} \leq$ -0.7 V, the photocurrent behaves like that of 70°C-treated s-MoO_x device in that it exhibits a smooth rise to steady-state. However, as the applied bias becomes more positive, the current overshoots steady-state and peaks before coming back down to a constant value. The magnitude of the peak increases with increasing applied voltage and takes longer to reach steady-state. For example, at V_{app} = +0.5 V, the current peaks to ~13 times its steady-state value and takes over 20μs to reach equilibrium. Based on the P3HT:PCBM vertical phase composition revealed by the DSIMS measurement, it is reasonable to posit that the peak in the transient stems from the fact that the active layer in the 150°C-MoO_x device is composed of mostly fullerene near the anode, which acts as a barrier to hole extraction. Initially, holes created near the anode are extracted but positive charges created away from the interface are not easily extracted. Instead, they are "blocked" by the fullerene phase and buildup within the film. As a result, a space charge is created that also inhibits the extraction of electrons at the cathode due to Coulombic attraction. Therefore, steady-state is established only after equilibration of the space charge and the enhanced charge recombination as a result of it.

The photocurrent decay of the 150°C-MoO_x device reveals an interesting phenomenon. As shown in the right inset of Fig. 5b, initially the decay slows down as the magnitude of the negative voltage bias is reduced from -1.5 V to -0.3 V. This is the slowing of the decay due to the reduction of the E-field. However, at $V_{app} \geq$ -0.2 V, the current initially decays quickly (and switches signs at more positive voltages) before slowly returning to zero. This occurs because when the light is turned off, the electrons near the cathode can leave the device very quickly which accounts for the sudden drop in current, during which time the internal electric field must readjust. However as the holes cannot come out due to the barrier for holes at the anode, electrons are then injected back into device to compensate for the space charge. Hence, the current goes to zero with opposite polarity for biases of $V_{app} \geq$ +0.1 V). The slow extraction/annihilation of holes accounts for the long tail in the decay of the transient.

3. The physical meaning of the photocurrent transients

To understand the physical origins of the changes in photocurrent signals of the devices with varying vertical blend composition as controlled with different s-MoO_x annealing temperatures, we performed a series of device simulations with and without a layer of PCBM close to the hole collecting contact. To simulate the device without the PCBM accumulation layer, an effective medium approximation was used where the LUMO and HOMO mobility edges were taken as −3.8 eV and −4.9 eV respectively. Between the HOMO and LUMO, electron and hole traps were introduced as an exponential distribution decaying away from the band edge. [21, 23] Poisson's equation and the bi-polar drift and diffusion equations were solved using a finite difference approach to describe electrostatic effects and carrier transport between the contacts. Carrier trapping and recombination within the device were described using the Shockley-Read-Hall recombination mechanism.[26, 27, 28, 29, 30] Both the electrical and optical models have been described in detail elsewhere. [21, 24, 25] To calibrate the model, it was fit to the experimental one-sun J-V curve and short-circuit pulsed data at 0.4 and 1.0 sun of the device without the

PCBM-rich layer. The resulting simulated and experimental steady-state J-V curves are plotted together in **Figure 6** and the simulated transient data is plotted in **Figure 7**. The model parameters are given in the SI.

To understand the influence of the PCBM buildup near the s-MoO_x interface, a 10-nm thick layer of PCBM was inserted into the simulation five nanometers away from the p-contact. To simplify interpretation of the results all material parameters of the pure PCBM layer (dielectric constant, electron and hole mobilities, etc.) were kept identical to that of the calibrated BHJ layer except for the HOMO level. The HOMO level was lowered until the simulated J-V curves in Figure 6 resembled those from the 150° C s-MoO_x device at varying light intensities. The distribution of carrier-trapped states is plotted in Figures 7a and 7b for the devices with and without the hole-blocking PCBM layer, respectively. The PCBM layer can be seen in Figure 7b as a small energetic step. Although the difference between the HOMO of P3HT and that of PCBM is around 1.5 eV, it was found that we only needed an energetic step 0.4 eV to reproduce the experimentally observed s-shaped J-V curves. This suggests there is some percolation of charge through the barrier due to remaining domains of P3HT, consistent with the DSIMS profile that revealed ~25% P3HT volume fraction in this region. It was found that when this energetic step was increased, the voltage at which the short-circuit current resembled that of a device without a blocking layer moved to more negative voltages. This is because a device with a larger barrier requires a larger negative potential to efficiently extract the carriers efficiently from it. Figure 7d shows the simulated photocurrent response of the device with the PCBM layer. It can be seen that the addition of this layer also generates photocurrent transients very close to those experimentally observed curves. This again suggests that the blocking layer is indeed the cause for the sharp spike at the beginning of the experimental transients and reduced steady-state current.

The transient data provides a measure of the recombination loss due to the presence of an effective barrier to extraction. **Figure 8** plots the simulated charge density and recombination rate from a device with and without the hole-blocking layer, Figs. 8a and 8b, respectively. It can be seen that in the device without the blocking layer, the transient oscillations die down after a few microseconds and the charge density levels off at around $2x10^{21}$ m^{-3}. In the device with the PCBM-rich layer, the charge density steadily climbs an order of magnitude higher to a value of $2x10^{22}$ m^{-3} within 200μs, and during this time the recombination rate also steadily increases. We now have enough information to explain the shape of the photocurrent transient from the device with the blocking layer. In a device with the PCBM layer, just after photo-excitation there is a high current spike because photo-generated electrons are initially free to produce current as the PCBM layer only blocks holes, furthermore around 50% of the holes generated are able to surmount the PCBM barrier and produce current. Thus, the maximum observed photocurrent is around 75% one would expect from a device without a hole-blocking layer. As time passes, the hole population between the blocking layer and *n*-contact steadily builds due to the presence of the barrier. This increasing excess hole population causes increasing recombination within the device and a reduction in electron photocurrent. As the carrier population within the device becomes stable, the photocurrent levels off. Thus, the difference between the peak of the photocurrent transient and the stable current can be thought of as an estimate of the recombination losses due to the blocking layer.

The experimental data for the device with the hole-blocking PCBM layer (Fig. 4b) shows that the

photocurrent spike broadens when the light intensity is reduced. We also observe this in the simulations (Fig. 7d). This effect can be explained by the fact that at a low light intensity there are fewer photo-generated carriers so it takes longer for the device to reach a stable carrier density, hence the broader peak observed at low light intensity. This is shown in detail in Figure S1 in the SI. As shown in SI Figure S2, simulations also confirm that a slow-down of the rise and fall in the photocurrent transients corresponds to either a low free carrier mobility or a high number of trap states. [Rod, where is the discussion/reference of Fig. S3?]

4. Conclusions

We have studied the current-voltage behavior of P3HT:PCBM BHJs with solution-processed MoO_x contact layers. We found that the solar cells have differing vertical composition in the active layer depending on the temperature used to sinter the s-MoO_x before the deposition of the P3HT:PCBM photo-active layer. If the s-MoOx is annealed at 150°C, PCBM segregates to the anode; but if 70°C is used instead, the P3HT:PCBM phase profile becomes more uniform. We used this processing control to identify the opto-electronic response signatures of the devices with contrasting phase profiles. Our work reveals the behavior of BHJs that have barriers to extraction of holes at the anode solely due to processing methods. Experimentally-measured and simulated microsecond photocurrent transients showed the device with PCBM accumulation at the s-MoOx hole-collecting interface displays a characteristic initial peak and subsequent reduction in photocurrent signal before reaching steady-state. Upon turn-off of the light, this device also showed unique decay dynamics in which the current dropped rapidly at first, then very slowly returned to zero.

Our results underscore the importance of understanding how the composition at solution-processed recombination layers may differ from the bulk due to processing conditions. The heat treatment of the metal oxide, necessary for increasing its electrical conductivity, can have indirect effects on the morphological behavior of organic blends films deposited onto it, independent of how the organic layer is subsequently treated.

The results here should aid in interpretation of non-ideal J-V characteristics for BHJs with novel electrode layers. The morphology of the active layer should always be investigated in parallel with device simulation to aid in identification of the origin of the J-V behavior that can be produced by multiple mechanisms. This may be of particular importance in multi-layer tandem solar cells in which metal oxides are now frequently used as recombination layers. In a tandem cell, the rates of hole and electron extraction at the front and back cells must be balanced by the recombination of charges in the interlayer(s) between the cells. It is therefore critical to avoid charge extraction barriers in either of the individual photoactive cells. And thus, if metal oxides are to be used as the recombination layer materials, care must be taken to ensure they are not an indirect cause of an undesirable distribution in the active-layer phase composition. We have presented a straightforward method for relating the photovoltaic response of the cell with the vertical composition profile of the photoactive layer.

5. Experimental Section

MoO_x *recipe and device fabrication*

[Taken from Jacek's manuscript...JACEK OR BTV TO RE-WRITE APPROPRIATELY] MAKE SURE THIS IS NOT IDENTICAL; REWORD AS NEEDED

"MoO_x precursor solutions were prepared by heating Molybdenum (VI) oxide bis(2,4-pentanedionate) (MoO2(acac)2, Alfa Aesar, 99%) directly in reagent grade methanol (Fischer Scientific) for 2 hours at 60°C in air, then aged for 2 days at room temperature. The precursor solutions were diluted to 23 mM (7.5 mg mL-1) and filtered (0.2 m PTFE filter) prior to use.

Solar cells were fabricated on ITO-coated glass substrates that was purchased from Thin Film Devices, Inc. The ITO-coated glass substrates were first cleaned with detergent, ultrasonicated in water, acetone and isopropyl alcohol, and UV-Ozone treated for 1 hour. Ambient $sMoO_x$ films were deposited onto ITO substrates in air by spin coating the precursor solutions at different concentrations and spin speeds to obtain the appropriate thicknesses. Thermal annealing was carried out in the glovebox. P3HT:PC61BM devices were fabricated by heating separate solutions of 30mg/mL P3HT (BASF) and 24 mg/mL PC61BM (Konarka Technologies) in chlorobenzene at 70 oC for 1 hour. Upon cooling to room temperature, equimolar amounts of each solution were combined and stirred for 30 minutes at room temperature. Solar cells were fabricated by filtering the final P3HT:PC61BM (15 mg mL- 1:12mg mL-1) solution through a 0.2 m PTFE filter onto the ITO/$sMoO_x$ substrates, then spin coating at 1500 RPM for 30 seconds.

Each device was completed by thermally evaporating aluminum cathodes (100 nm) through a shadow mask under a vacuum of about 8 106 torr. The active area of the devices was either 19.60 mm2 or 4.5 mm2. During the measurement, an aperture with the area of 12.38 mm2 was used for the 19.60 mm2 devices. Device performances for both active areas were similar. Current density-voltage (J-V) characteristics were measured using a Keithley 236 Source Measure Unit. Solar cell performance used an Air Mass 1.5 Global (AM 1.5 G) solar simulator with an irradiation intensity of 100 mW cm-2. IPCE spectra were measured by using a QE measurement system (PV measurements, Inc.). The integrated IPCE values were always within a few percent of the measured short-circuit current densities."

Dynamic Secondary-ion Mass Spectroscopy (DSIMS)

[Taken from Neal's Adv. Energy Mater. paper on P3HT/PCBM interdiffusion...NEIL OR JACEK TO RE-WRITE APPROPRIATELY]

"A Physical Electronics 6650 Quadropole dynamic SIMS was used to obtain depth profiles of the films. The substrates were cooled on a cryostage for 30 min prior to analysis. A 2kV O2+ beam at 45 nA was rastered across a 200 m 200 m area, of which only the middle 15% was analyzed for composition by collecting negative secondary ions"

Pulsed LED Transient

We used pulsed LED illumination to study the transient photocurrent response of polymer:fullerene photovoltaics, in a manner similar to previous work.[8]1 The solar cells were subjected to a square-pulse optical excitation provided by an array of fast-switching LEDs with an output wavelength centered around 625 nm. A pulse duration of 500 μs was chosen in order to ensure the photocurrent attained steady-state. The "off-time" between pulses was one second so

that all photo-generated carriers had ample time to exit the device before the next excitation pulse. Photocurrent transients were measured as a function of excitation light intensity and applied voltage bias.

To set the light intensity of the LED array to "1 sun equivalent", we first measured Jsc of the solar cells using a calibrated AM1.5 solar simulator. Next, we adjusted the power supply controlling the LEDs until the Jsc under illumination from the LEDs matched the Jsc measured with the solar simulator.

Supporting Information ((delete if not applicable))
Supporting Information is available online from the Wiley Online Library or from the author.

Acknowledgements
MLC and BTdV were supported as part of the Center for Energy Efficient Materials, an Energy Frontier Research Center funded by the U.S. Department of Energy, Office of Science, Office of Basic Energy Sciences under Award Number DE-SC0001009. NDT acknowledges support from the NSF ConvEne IGERT Program (NSF-DGE 0801627), and NSF Graduate Research Fellowship. Portions of this research were carried out at the MRL Central Facilities, which is supported by the MRSEC Program of the NSF under Award No. DMR-1121053; a member of the NSF-funded Materials Research Facilities Network (www.mrfn.org).

Received: ((will be filled in by the editorial staff))
Revised: ((will be filled in by the editorial staff))
Published online: ((will be filled in by the editorial staff))

1. M. A. Green, K. Emery, Y. Hishikawa, W. Warta, and E. D. Dunlop. Progress in Photovoltaics: Research and Applications, 2012, 20 1 12–20.
2. C. J. Emmott, A. Urbina and J. Nelson, Sol. Energy Mater. Sol. Cells, 2012, 97, 14–21.
3. Song Chen, Jesse R. Manders, Sai-Wing Tsang, and Franky So. Metal oxides for interface engineering in polymer solar cells. J. Mater. Chem., 22:24202–24212, 2012.
4. M. M. Voigt, R. C. Mackenzie, C. P. Yau, P. Atienzar, J. Dane, P. E. Keivanidis, D. D. Bradley and J. Nelson, Sol. Energy Mater. Sol. Cells, 2011, 95(2), 731–734.
5. Scott R. Hammond, Jens Meyer, N. Edwin Widjonarko, Paul F. Ndione, Ajaya K. Sigdel, Andres Garcia, Alexander Miedaner, Matthew T. Lloyd, Antoine Kahn, David S. Ginley, Joseph J. Berry, and Dana C. Olson. Low-temperature, solution-processed molybdenum oxide hole-collection layer for organic photovoltaics. J. Mater. Chem., 22:–, 2012.
6. Jacek J. Jasieniak, Jason Seifter, Jang Jo, Tom Mates, and Alan J. Heeger. A solution processed MoO x anode interlayer for use within organic photovoltaic devices. Adv. Funct. Mater., 22(12):2594–2605, 2012
7. M. M. Voigt, R. C. Mackenzie, S. P. King, C. P. Yau, P. Atienzar, J. Dane, P. E. Keivanidis, I. Zadrazil, D. D. Bradley and J. Nelson, Sol. Energy Mater. Sol. Cells, 2012, 105, 77–85.
8. G. Juska, K. Arlauskas, M. Viliunas, K. Genevicius, R. Osterbacka, and H. Stubb. Charge transport in pi -conjugated polymers from extraction current transients. Phys. Rev. B, 62(24):R16235, 2000.

9. [Refs needed; Brady, M. et al., Soft Matter, 2011?].
10. A. J. Mozer, G. Dennler, N. S. Sariciftci, M. Westerling, A. Pivrikas, R. Osterbacka,and G. Juska. Time-dependent mobility and recombination of the photoinduced charg carriers in conjugated polymer/fullerene bulk heterojunction solar cells. Phys. Rev. B, 72(3):035217–10, Jul 2005.

11. A. Pivrikas, N. S. Sariciftci, G. Juska, and R. Osterbacka. A review of charge transportand recombination in polymer/fullerene organic solar cells. Progress in Photovoltaics,15(8):677–696, Dec 2007.

12. Bertrand Tremolet de Villers, Christopher J. Tassone, Sarah H. Tolbert, and Benjamin J. Schwartz. Improving the reproducibility of P3HT:PCBM solar cells by controlling the PCBM/cathode interface. J. Phys. Chem. C, 113(44):18978–18982, November 2009.

13. Christopher G. Shuttle, Neil D. Treat, Jessica D. Douglas, Jean M. J. Fr´echet, and Michael L. Chabinyc. Deep energetic trap states in organic photovoltaic devices. Adv. Energy Mater., 2:111–119, 2011.

14. Christopher R. McNeill, Inchan Hwang, and Neil C. Greenham. Photocurrent transients inall-polymer solar cells: Trapping and detrapping effects. J. Appl. Phys., 106(2):024507–8, 2009.

15. Zhe Li and Christopher R. McNeill. Transient photocurrent measurements of PCDTBT:PC 70 BM and PCPDTBT:PC 70 BM solar cells: Evidence for charge trapping in efficient polymer/fullerene blends. J. Appl. Phys., 109(7):074513, 2011.

16. Zhe Li, Feng Gao, Neil C. Greenham, and Christopher R. McNeill. Comparison of the operation of polymer/fullerene, polymer/polymer, and polymer/nanocrystal solar cells: A transient photocurrent and photovoltage study. Adv. Funct. Mater., 21(8):1419–1431,2011.
17. Jenny Nelson, James Kirkpatrick, and P. Ravirajan. Factors limiting the efficiency of molecular photovoltaic devices. Phys. Rev. B, 69(3):035337–, January 2004.
18. Wolfgang Tress, Annette Petrich, Markus Hummert, Moritz Hein, Karl Leo, and Moritz Riede. Imbalanced mobilities causing S-shaped IV curves in planar heterojunction organic solar cells. Appl. Phys. Lett., 98(6):063301, 2011.
19. M. Glatthaar, M. Riede, N. Keegan, K. Sylvester-Hvid, B. Zimmermann, M. Niggemann, A. Hinsch, and A. Gombert. Efficiency limiting factors of organic bulk heterojunction solar cells identified by electrical impedance spectroscopy. Sol. Energy Mater. Sol. Cells, 91(5):390–393, 2007.
20. Dhritiman Gupta, Monojit Bag, and K. S. Narayan. Correlating reduced fill factor in polymer solar cells to contact effects. Appl. Phys. Lett., 92(9):093301–3, 2008.
21. [Refs needed, Kniepert, J. Phys. Chem. Lett., 2011 and/or Deibel, PRL, 103, 2009]
22. Roderick C. I. MacKenzie, Thomas Kirchartz, George F. A. Dibb, and Jenny Nelson. Modeling nongeminate recombination in p3ht:pcbm solar cells. J. Phys. Chem. C, 0(0), 2011.
23. Jenny Nelson. Diffusion-limited recombination in polymer-fullerene blends and its

influence on photocurrent collection. Phys. Rev. B, 67(15):155209, Apr 2003.
24. Roderick C. I. MacKenzie, Christopher G. Shuttle, Michael L. Chabinyc, and Jenny Nelson. Extracting microscopic device parameters from transient photocurrent measurements of P3HT:PCBM solar cells. Adv. Energy Mater., 2:662–669, 2012.
25. Felix Deschler, Daniel Riedel, Bernhard Ecker, Elizabeth von Hauff, Enrico Da Como, and Roderick C. I. MacKenzie. Increasing organic solar cell efficiency with polymer interlayers. Phys. Chem. Chem. Phys., 15:764–769, 2013.
26. C. Groves and N. C. Greenham. Bimolecular recombination in polymer electronic devices. Phys. Rev. B, 78(15):155205–8, 2008.
27. Maria Hilczer and M. Tachiya. Unified theory of geminate and bulk electron–hole recombination in organic solar cells. The Journal of Physical Chemistry C, 114(14):6808–6813, 2010.
28. L. J. A. Koster, V. D. Mihailetchi, and P. W. M. Blom. Bimolecular recombination in polymer/fullerene bulk heterojunction solar cells. Applied Physics Letters, 88(5):052104, 2006.
29. R. A. Street. Localized state distribution and its effect on recombination in organic solar cells. Phys. Rev. B, 84(7):075208, Aug 2011.
30. A. Wagenpfahl, C. Deibel, and V. Dyakonov. Organic solar cell efficiencies under the aspect of reduced surface recombination velocities. Selected Topics in QuantumElectronics, IEEE Journal of, 16(6):1759 –1763, nov.-dec. 2010.
31. Hwang, Christopher R. McNeill, and Neil C. Greenham. Drift-diffusion modeling of photocurrent transients in bulk heterojunction solar cells. Journal of Applied Physics, 106(9):094506, 2009.

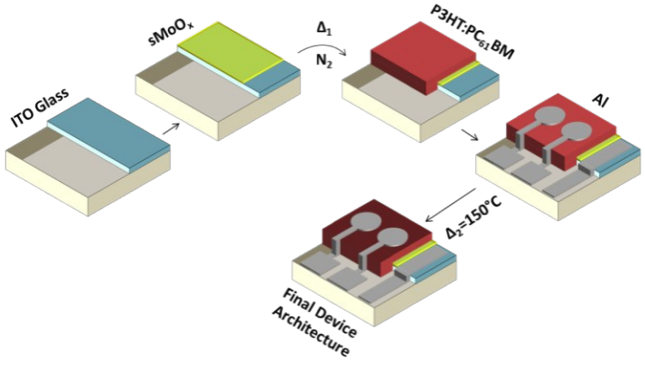

Figure 1. Schematic of s-MoO_x BHJ solar cell preparation. Δ_1 represents the heat-treatment temperature of the s-MoO_x layer before subsequent deposition of the P3HT:PCBM active layer. In this work, we used two different Δ_1 temperatures—70°C and 150°C—yielding contrasting P3HT:PCBM vertical phase compositions. Using Δ_1 =70°C results in a mostly-homogenous distribution of P3HT and PCBM, whereas Δ_1 =150°C results in a PCBM-rich accumulation layer near the s-MoO_x hole-contact layer. [Can we use this figure in this article if it's also going to be used in Jacek's article? If not, I can try to make a similar, but different, version.]

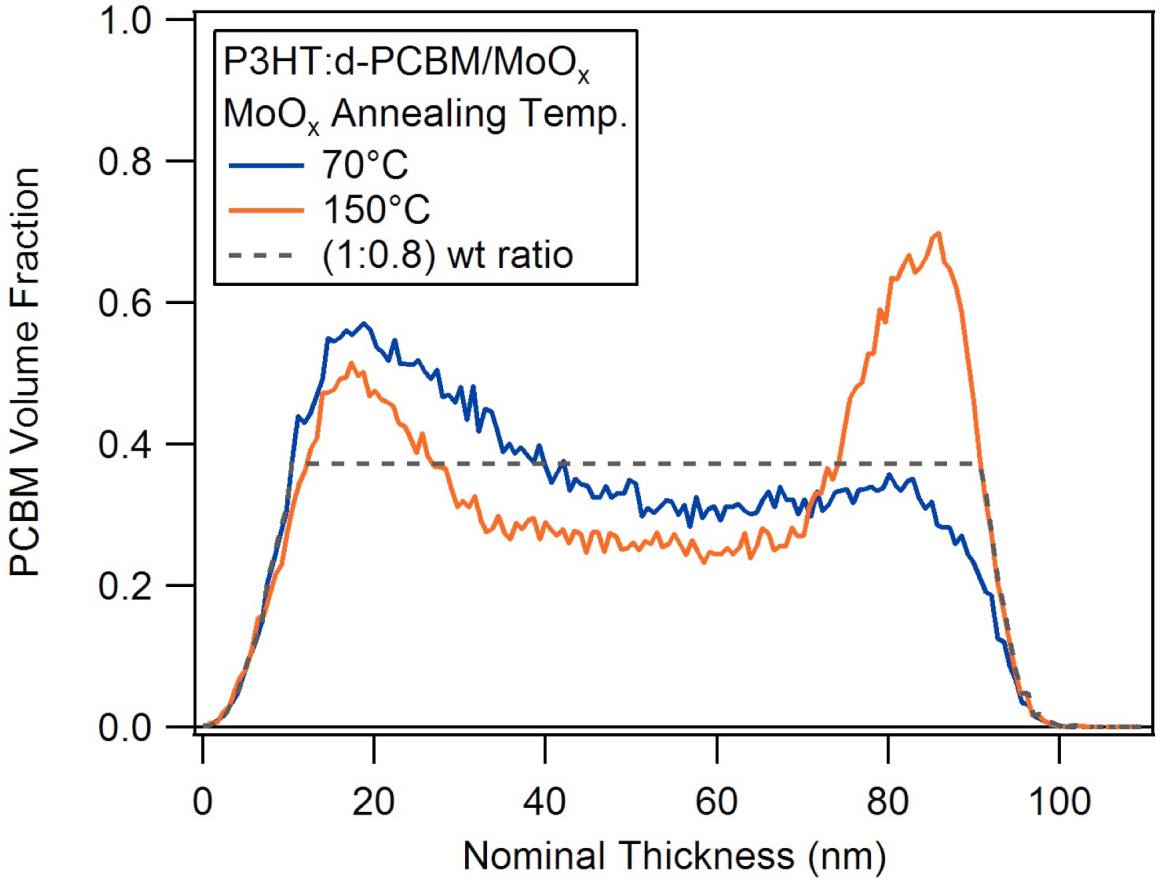

Figure 2. DSIMS profile of a P3HT:PCBM bulk-heterojunction film deposited on top of a solution-processed MoO_x hole-contact layer. The s-MoO_x was thermally treated at 70°C (blue trace) or 150°C (orange trance) before deposition of the BHJ film. Heating of the s-MoO_x to 150°C leads to a subsequent accumulation of PCBM at the oganic-layer/s-MoO_x interface. The grey dashed line represents the PCBM volume fraction if it were uniformly distributed with P3HT in a 1:0.8 wt. ratio film.

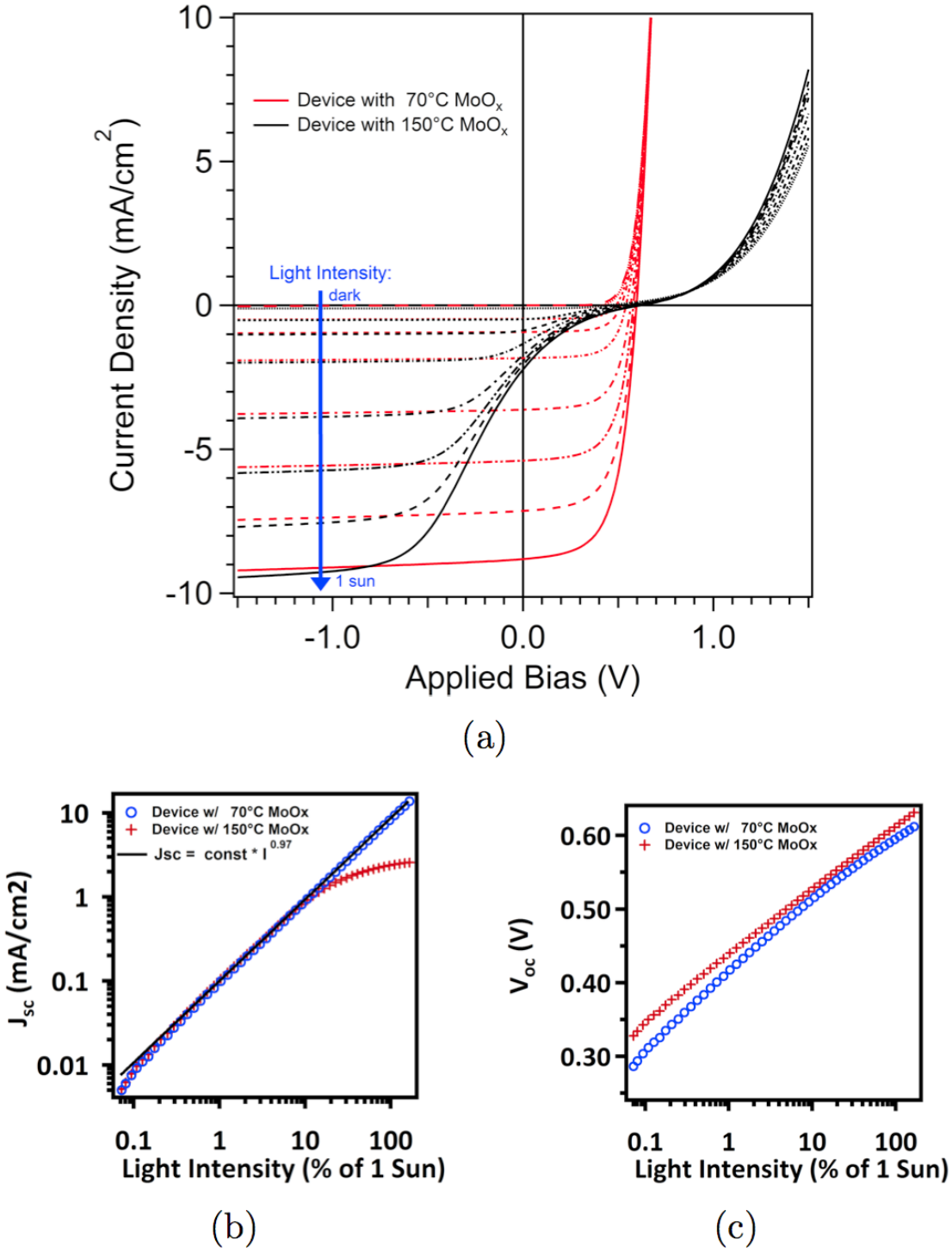

Figure 3. (a) Light-intensity dependence of the steady-state J-V curve for devices with MoO_x anode interlayers treated at 70 ◦C (red curves) and 150 ◦C (black curves). Light-intensity dependence of short-circuit current density, Jsc (b) and open-circuit voltage, Voc (c). The curve fit in (b) shows $J \propto I\alpha$, with $\alpha = 0.97$.

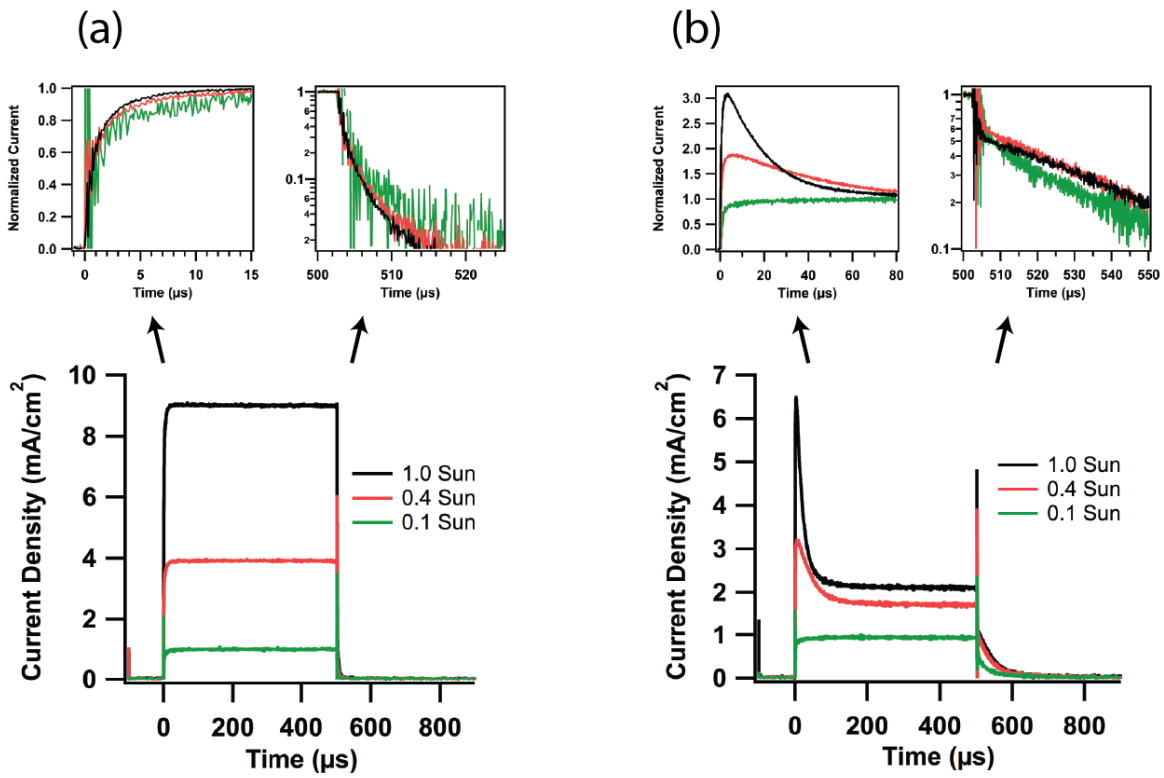

Figure 4. Photocurrent transients at short-circuit current condition for three different light intensities: 100, 40, and 10% of one-sun equivalent (See Experiment section in the main text for more details of one-sun equivalence). Transients are shown for (a) 70◦C- and (b) 150◦C-MoO_x devices. The rise and decay of the photocurrent following turn-on and turn-off, respectively, of the light pulse are shown in the insets above the full photocurrent traces. In the insets, the traces have been normalized to the mean value of the current from 450–500μs when steady-state has been established. Samples were illuminated with an array of fast-switching LEDs centered at 625 nm. Time = 0 is set to the onset of the 500-μs light pulse.

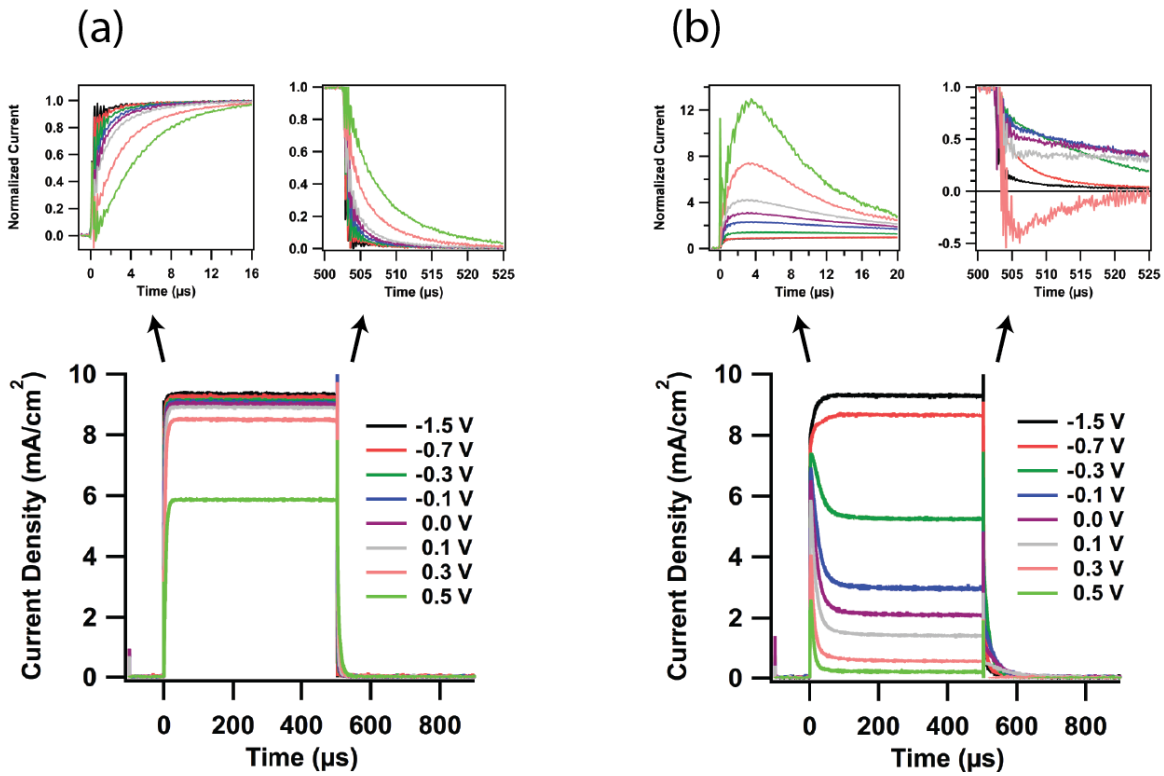

Figure 5. Photocurrent transients as a function of applied voltage bias at illumination intensity equivalent to one sun. Transients are shown for (a) 70 ◦C- and (b) 150◦C-MoO_x devices. The rise and decay of the photocurrent following turn-on and turn-off, respectively, of the light pulse are shown in the insets above the full photocurrent traces. In the insets, the traces have been normalized to the mean value of the current from 450–500μs when steady-state has been established. Samples were illuminated with an array of fast-switching LEDs centered at 625 nm. Time = 0 is set to the onset of the 500-μs light pulse.

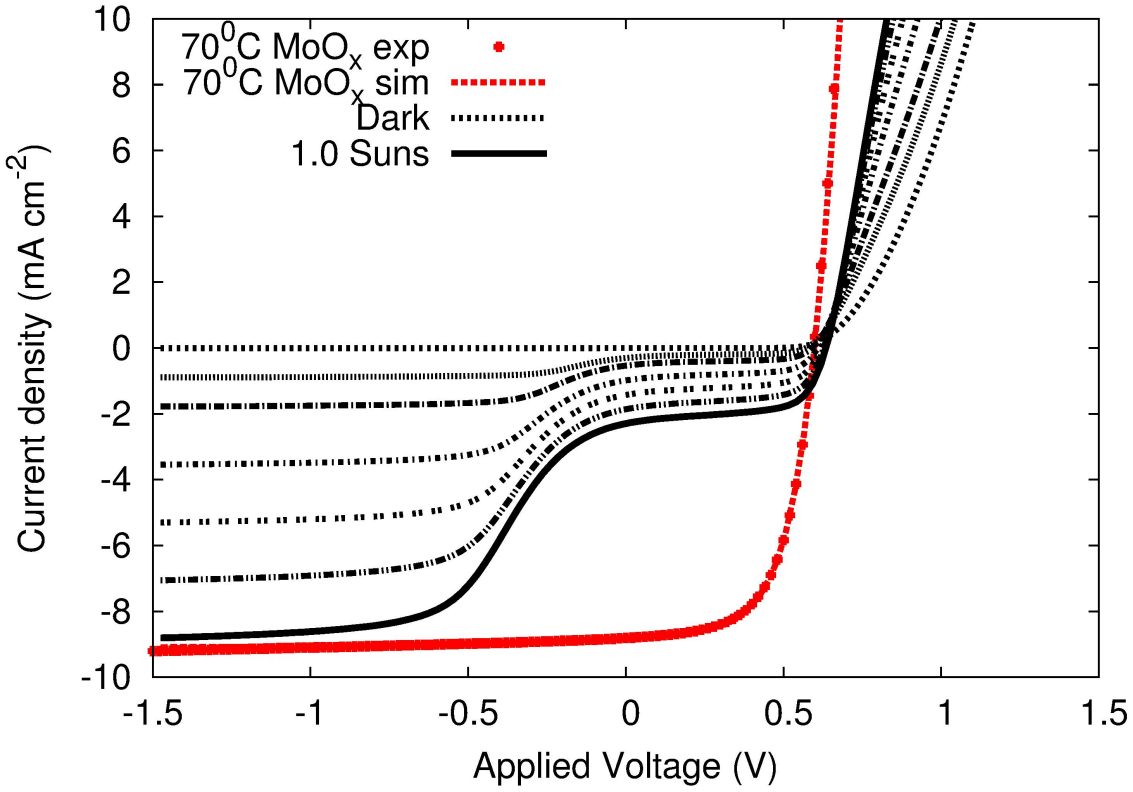

Figure 6. A fit of the model (red lines) to the experimental light JV curve (red points) from the MoO_x device annealed at 70^{O}C with no PCBM blocking layer. Predicted steady-state J-V curves when a 10-nm wide PCBM layer is introduced into the simulation 5 nm away from the *p*-contact.

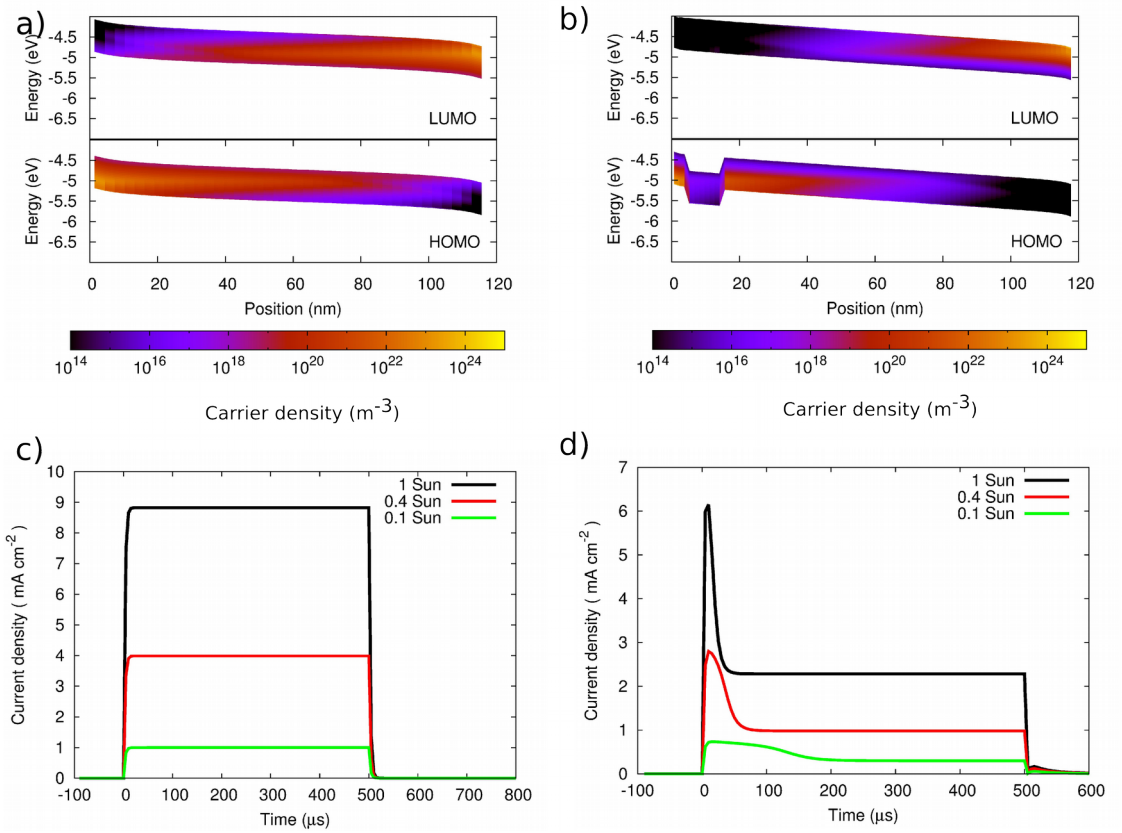

Figure 7. a) The distribution of trapped carriers within a P3HT:PCBM device in the dark at short circuit; the shading represents the density of carriers trapped within the exponential tail of trap states. b) The distribution of trapped carriers within a P3HT:PCBM device with a 10-nm hole-blocking PCBM layer inserted 5 nm from the hole collecting contact in the dark at short circuit; the step in the HOMO represents the deeper HOMO of the PCBM molecule. The corresponding simulated electrical response to a 500-µs optical excitation of a device c) in the absence of and d) including a hole-blocking PCBM layer near the *p*-contact.

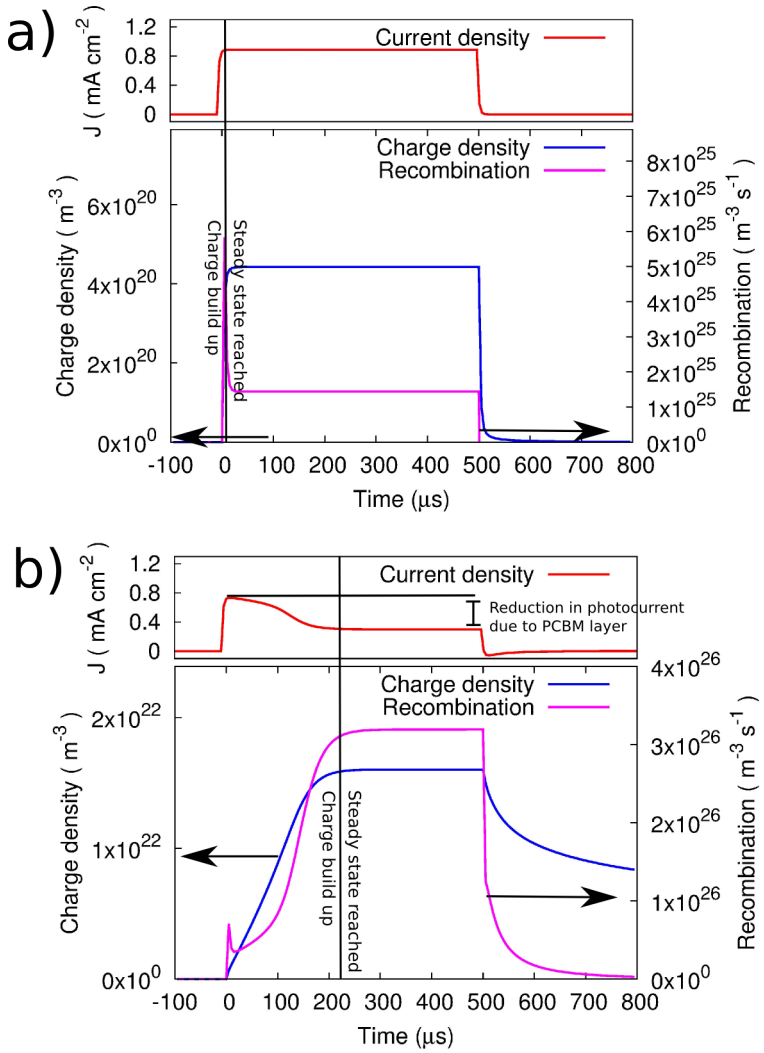

Figure 8. a): (top) Simulated photocurrent transient without PCBM blocking layer and (bottom) corresponding charge density and recombination rate. b) (top) Simulated photocurrent transient with the 10-nm thick PCBM layer near the p-contact and (bottom) corresponding charge density and recombination rate. The introduction of the blocking layer increases the charge density within the device reducing the photocurrent.

The table of contents entry should be fifty to sixty words long (max. 400 characters), and the first phrase should be bold. The entry should be written in the present tense and impersonal style. The text should be different from the abstract text.

Keyword (see list)

C. Author-Two, D. E. F. Author-Three, A. B. Corresponding Author* ((same order as byline))

Title ((no stars))

ToC figure ((Please choose one size: 55 mm broad × 50 mm high **or** 110 mm broad × 20 mm high. Please do not use any other dimensions))

((Supporting Information can be included here using this template))

Supporting Information

for *Adv. Energy Mater.*, DOI: 10.1002/aenm.((please add manuscript number))

Vertical Composition and Transient Photocurrent Dynamics in Organic Solar Cells with Solution-processed MoO_x Contact Layers

Bertrand J. Tremolet de Villers, Roderick C. I. MacKenzie, Jacek J. Jasieniak, Neil Treat, Alan Heeger, and Michael Chabinyc*

E-mail: mchabinyc@engineering.ucsb.edu

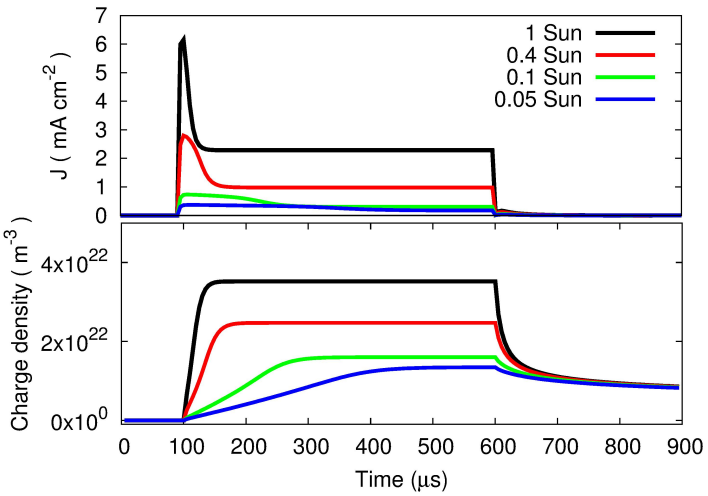

Figure S1: Photucurrent pulses (J) plotted against charge density within the device. It can be seen that the lower the light intensity the longer it takes for the charge density (and thus recombination rate) to reach steady state. Thus a narrow photocurrent spike corresponds to a high light intensity and rapid rise in the recombination rate.

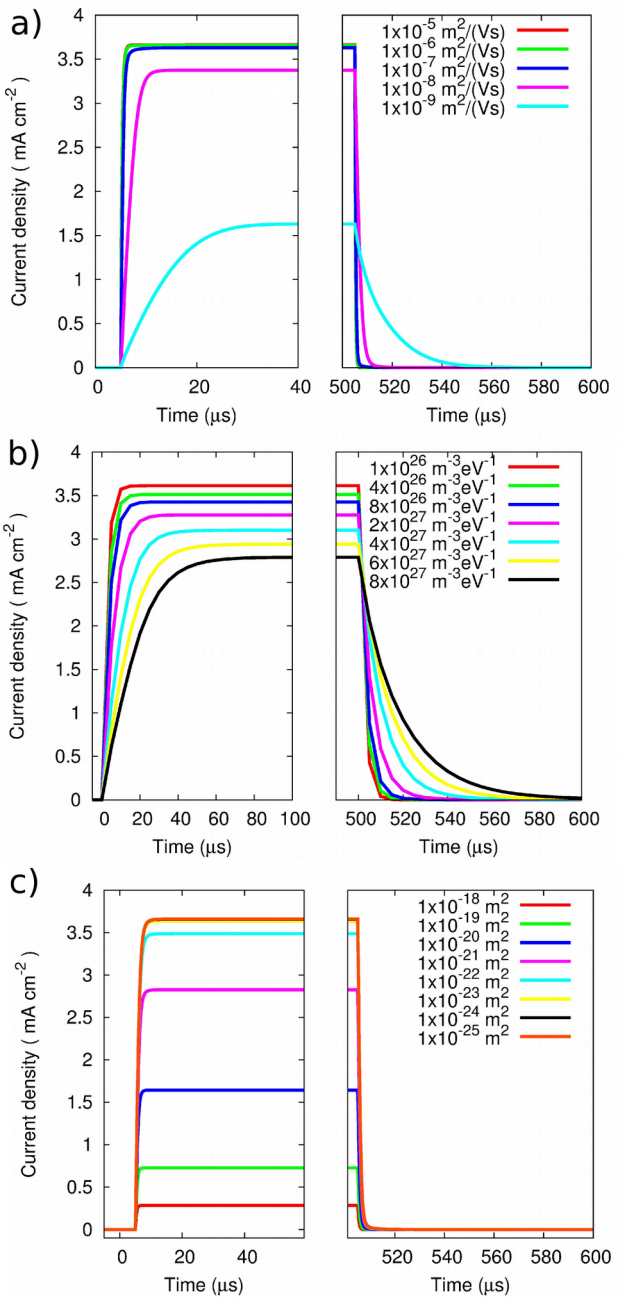

Figure S2: Photocurrent transients at 0.4 Suns; a) variation of transient with mobility; b) variation of transient with trap density; and c) variation of transient with recombination cross-section. The fewer traps there are and the higher the mobility the faster the device reaches steady state.

Band bending and electrostatic effects:

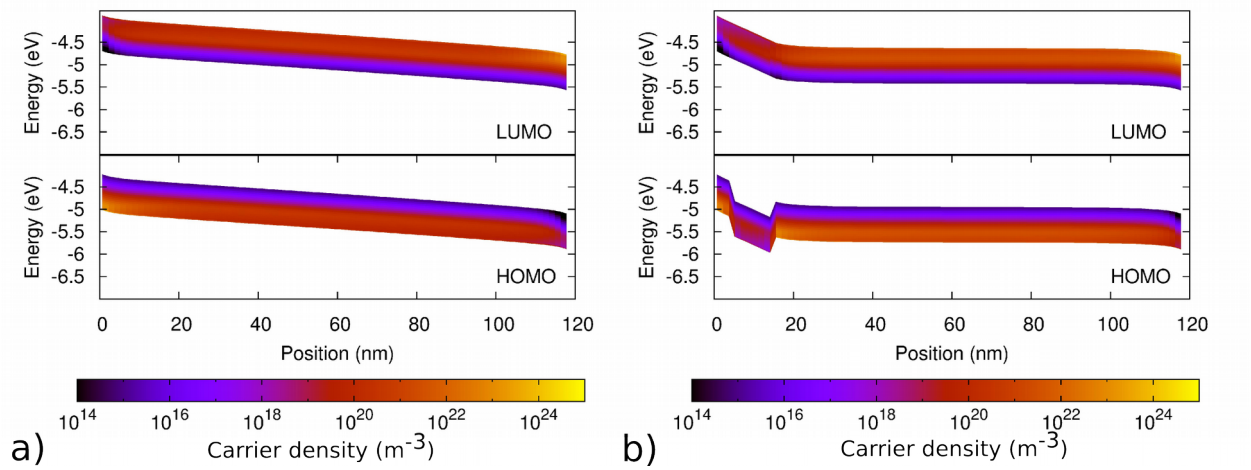

Figure S3: Distribution of trapped carriers in energy space at short circuit at 1.0 Sun for a) the device with no blocking layer; and b) the device with a 10-nm hole-blocking PCBM layer. In (b), the carrier distribution between 15 nm and 120 nm in the device with a blocking layer is effectively flat. This is because the blocking layer causes a large buildup of holes in this region, the holes attract an equal number of electrons through electrostatic attraction, thus the net charge is zero meaning there is no potential drop. Therefore in this region, drift no longer drives carriers out of the device making transport less efficient. Flat bands are therefore a secondary negative effect of having a carrier blocking layer.